J. Fluid Mech. (2006), *vol.* 550, *pp.* 149–173.
doi:10.1017/S0022112005007998 Printed in the United Kingdom

Interfacial conditions between a pure fluid and a porous medium: implications for binary alloy solidification

By M. LE BARS AND M. GRAE WORSTER

Institute of Theoretical Geophysics, Department of Applied Mathematics and Theoretical Physics, University of Cambridge, Wilberforce Road, Cambridge, CB3 0WA, UK

(Received 17 December 2004 and in revised form 8 August 2005)

The single-domain Darcy–Brinkman model is applied to some analytically tractable flows through adjacent porous and pure-fluid domains and is compared systematically with the multiple-domain Stokes–Darcy model. In particular, we focus on the interaction between flow and solidification within the mushy layer during binary alloy solidification in a corner flow and on the effects of the chosen mathematical description on the resulting macrosegregation patterns. Large-scale results provided by the multiple-domain formulation depend strongly on the microscopic interfacial conditions. No satisfactory agreement between the single- and multiple-domain approaches is obtained when using previously suggested conditions written directly at the interface between the liquid and the porous medium. Rather, we define a viscous transition zone inside the porous domain, where the Stokes equation still applies, and we impose continuity of pressure and velocities across it. This new condition provides good agreement between the two formulations of solidification problems when there is a continuous variation of porosity across the interface between a partially solidified region (mushy zone) and the melt.

1. Introduction

Simultaneous flow through both a pure fluid and a porous medium occurs in a wide range of industrial processes and natural phenomena. It happens for instance during the solidification of multi-component melts, where the solid and the remaining liquid are separated by a layer of mixed phase called a mushy layer that continuously evolves because of internal solidification and local dissolution (see reviews by Worster 1997, 2000, for example).

A classical approach to such systems (either with a reacting or a non-reacting porous matrix) consists of solving the Navier–Stokes equations in the fluid and Darcy's equation in the porous medium (e.g. Levy & Sanchez-Palencia 1975; Schulze & Worster 1999). The problem then remains of defining relevant boundary conditions at the interface between the two domains. Continuity of pressure and normal velocity (i.e. mass conservation) are robust and generally accepted boundary conditions. Then, naïve choices regarding the tangential velocity component would be either that it vanishes for low permeability or that it is continuous for large permeability. However, both turn out to be inaccurate, as shown for instance by the experiments of Beavers & Joseph (1967). Rather, these authors postulated a discontinuity in the interfacial

tangential velocity given by

$$u_S - u_D = \frac{\sqrt{\Pi}}{\alpha}\frac{\partial u_S}{\partial z}, \tag{1.1}$$

where z is the direction perpendicular to the interface, u_S the Stokes velocity calculated inside the fluid, u_D the Darcy velocity calculated inside the porous matrix and Π its permeability. The dimensionless coefficient α characterizes the structure of the permeable material near its interface with the pure liquid, and must therefore be determined for each particular system. This boundary condition was validated experimentally by Beavers & Joseph (1967) in the case of a Poiseuille flow in a channel formed by an impermeable wall at $z=+h$ and a permeable wall at $z=0$ (cf. figure 1 below). It was also justified analytically by Saffman (1971) using *ad hoc* representations of forces and energy exchanges at the interface. Since then, more complicated multiple-domain formulations have been suggested, introducing a fluid–fluid viscous correction in the porous matrix (Brinkman 1947). Many types of interfacial conditions have been used, e.g. continuity of the tangential velocity but discontinuity of the tangential shear stress (Ochoa-Tapia & Whitaker 1995*a*), or continuity of both the tangential velocity and the tangential shear stress (Neale & Nader 1974), or discontinuity of both the tangential velocity and the tangential shear stress (Cieszko & Kubik 1999). Clearly the definition of practical and relevant first-order interfacial conditions between a pure fluid and a porous matrix remains an open question.

To avoid these problems computationally, some models of binary alloy solidification use single formulations for the solid, the liquid and the mushy layer, which are then resolved on the same mesoscopic scale (see for instance Felicelli, Heinrich & Poirier 1991; Schneider *et al.* 1997). This approach seems to eliminate the need for explicit consideration of interfaces. Mesoscopic transport equations are either postulated using mixture theory (Hills, Loper & Roberts 1983) or derived from the volume averaging of the classical microscopic equations (Beckermann & Viskanta 1988). Until now, this single-domain method has been utilised mostly to determine the various characteristic fields (temperature, concentration, liquid fraction, velocity) at a mesoscopic scale in industrial settings (e.g. Gu & Beckermann 1999), whereas the multiple-domain method has been utilised to study the dynamics of interactions between the different regions in idealized theoretical cases (e.g. Chung & Worster 2002). Results from the two approaches have been compared in the case of the linear stability analysis of double-diffusive convection in superposed fluid and porous layers (Zhao & Chen 2001).

In the present paper, we apply the single-domain formulation to some analytically tractable cases and systematically compare it with the multiple-domain formulation, using previously suggested interfacial conditions as well as a new set proposed here. Our purposes are to illustrate how large-scale results are influenced by the assumed small-scale structure of the interface and to suggest under which conditions results provided by the two approaches agree. Our main interest stems from modelling interactions between flow and solidification within mushy layers.

In § 2, we derive the single-domain equation of motion (i.e. Darcy–Brinkman) using the volume-averaging method, in a context in which all variables change on scales larger than the averaging length. We highlight the underlying assumptions, define the relevant parameters and variables, and study its limits in the case of either a pure fluid or a small Darcy number, where it respectively gives rise to the Navier–Stokes and Darcy equations. In § 3, we solve the Darcy–Brinkman equation

in the configuration studied by Beavers & Joseph (1967): a Poiseuille flow in a fluid overlying a porous layer with a constant porosity. This allows us to define a new set of conditions at the mushy layer–liquid interface, which leads to a closer agreement with the experiments of Beavers & Joseph (1967) compared to the previously proposed interfacial conditions. In § 4, we similarly study a corner flow in a fluid overlying a porous layer, both with a constant porosity and with a linear porosity variation. In addition to the previous case, these self-similar configurations allow us, still with one-dimensional calculations, to take into account the effects of flow crossing the interface. Differences between the various formulations are then highlighted. Finally, in § 5, we study the solidification of a binary alloy in a corner flow. The interaction between flow and solidification within the mushy region is examined precisely in this simple geometry, and the importance of the interfacial conditions is highlighted by comparing their effects on the computed macroscopic fields (i.e. temperature, velocity, porosity and, especially, bulk concentration).

2. The Darcy–Brinkman equation and its limits

The Darcy–Brinkman equation has been widely used to study flows in porous media in various contexts. However, a careful look at the publications over the past twenty years shows no general agreement regarding its conditions of applicability and the definition of its variables, especially the 'effective' viscosity and the relevant pressure. Hence, we present here a concise derivation of the Darcy–Brinkman equation based on the volume-averaging method, focusing on the underlying assumptions and on its relationships with the Navier–Stokes and Darcy equations. We focus our attention on cases in which all variables are continuous at the mesoscopic scale (for instance in solidification problems). A complete mathematical description of cases in which the porosity is discontinuous can be found in Ochoa-Tapia & Whitaker (1995*a*).

2.1. *A volume-averaged mesoscopic momentum-transport equation*

We consider a domain comprising both a solid and a liquid phase, for instance a porous medium or a solidifying material, and we define a mesoscopic volume ΔV large enough to smooth the morphological complexities but small enough to capture the global transport properties (i.e. typically a few pore lengths). We denote by η the viscosity of the liquid, χ the liquid volume fraction (porosity) and ρ_k the density of the liquid ($k = l$) and the solid ($k = s$) respectively. For simplicity, we suppose that the solid phase is stationary, i.e. $\boldsymbol{u}_s = \boldsymbol{0}$, and we neglect variations of material properties inside the control volume ΔV, i.e. $[\eta]^l = \eta$ and $[\rho_k]^k = \rho_k$, where $[\rho_k]^k$ stands for the intrinsic volume average in phase k (see the Appendix).

The microscopic momentum equation inside the fluid phase is the Navier–Stokes equation

$$\frac{\partial}{\partial t}\rho_l \boldsymbol{u}_l + \nabla\cdot(\rho_l \boldsymbol{u}_l \boldsymbol{u}_l) = -\nabla P_l + \nabla\cdot\boldsymbol{T} + \rho_l \boldsymbol{g}, \tag{2.1}$$

where $\boldsymbol{u}_l$ is the liquid velocity, P_l the pressure inside the liquid, $\boldsymbol{g}$ the acceleration due to gravity, and $\boldsymbol{T}$ the viscous stress tensor. We consider here a Newtonian fluid, where

$$\boldsymbol{T} = \eta(\nabla \boldsymbol{u}_l + (\nabla \boldsymbol{u}_l)^T). \tag{2.2}$$

The mesoscopic momentum equation can be obtained by taking the average of (2.1) over ΔV, using concepts and formulae defined in the Appendix. Hence,

$$\frac{\partial}{\partial t}[\rho_l \boldsymbol{u}_l] + \nabla\cdot(\chi\,[\rho_l \boldsymbol{u}_l]^l [\boldsymbol{u}_l]^l) = -[\nabla P_l] + \nabla\cdot[\boldsymbol{T}] + [\rho_l \boldsymbol{g}] + M_l + A_l + I_l, \tag{2.3}$$

where

$$M_l = -\nabla \cdot [\hat{\boldsymbol{u}}_l \hat{\boldsymbol{u}}_l], \tag{2.4a}$$

$$A_l = \frac{1}{\Delta V} \int_{\Delta A} \boldsymbol{u}_l (\boldsymbol{w} - \boldsymbol{u}_l) \cdot \boldsymbol{n}_l \, \mathrm{d}A, \tag{2.4b}$$

$$I_l = \frac{1}{\Delta V} \int_{\Delta A} \boldsymbol{T} \cdot \boldsymbol{n}_l \, \mathrm{d}A. \tag{2.4c}$$

Here, $[\boldsymbol{u}_l]$ stands for the average value of the liquid velocity over ΔV, $\hat{\boldsymbol{u}}_l$ for its fluctuating component, $\boldsymbol{w}$ for the velocity of the microscopic interface and ΔA for the interfacial area between the liquid and solid phases in ΔV (see the Appendix).

We can simplify the various terms on the right-hand side as follows. According to (A3) in the Appendix.

$$[\nabla P_l] = \chi \nabla [P_l]^l + \frac{1}{\Delta V} \int_{\Delta A} \hat{P}_l \boldsymbol{n}_l \, \mathrm{d}A, \tag{2.5}$$

and we neglect the second term, corresponding to pressure fluctuations on the solid–liquid interface. We should highlight here that $[P_l]^l$ (i.e. the average value of the liquid pressure in the liquid only) is the relevant physical parameter: it could for instance be measured experimentally by placing an open pipe filled with pure fluid within the porous structure. Hence, at an interface of a porous matrix, we expect this pressure to be continuous with the pressure in the adjacent pure fluid.

Also from (A3) of the Appendix,

$$[\eta \nabla \boldsymbol{u}_l] = \eta \nabla [\boldsymbol{u}_l] + \frac{\eta}{\Delta V} \int_{\Delta A} \boldsymbol{n}_l \boldsymbol{u}_l \, \mathrm{d}A. \tag{2.6}$$

Here, the second term on the right-hand side accounts for the influence of the liquid–solid interface geometry on the large-scale momentum diffusion. When $\boldsymbol{u}_l$ is uniform, this term should be zero, so it is related to leading order by $\nabla[\boldsymbol{u}_l]$. Taking it proportional to $\nabla[\boldsymbol{u}_l]$ as a first-order approximation, one can define an effective viscosity η^* as

$$[\eta \nabla \boldsymbol{u}_l] = \eta^* \nabla [\boldsymbol{u}_l] \tag{2.7}$$

(e.g. Shyy *et al.* 1997). Hence,

$$\nabla \cdot [\boldsymbol{T}] = \nabla \cdot \eta^* (\nabla [\boldsymbol{u}_l] + (\nabla [\boldsymbol{u}_l])^{\boldsymbol{T}}). \tag{2.8}$$

However, in the following, we consider either a fixed non-reacting solid matrix or a mushy layer in which $\rho_l = \rho_s$. Then the liquid velocity at the microscopic liquid–solid interface is zero and (2.6) implies $\eta^* = \eta$. In these cases, the effective viscosity should not be taken as an adjustable coefficient, conveniently chosen to match expected results.

The term M_l appears because $\boldsymbol{u}_l$ fluctuates inside the control volume and thus differs from its averaged value. Following large-eddy-simulation techniques in turbulence (e.g. Lesieur 1993; Moin *et al.* 1991), these fluctuations could be parameterized and related to the mesoscopic gradient of velocity (e.g. Shyy *et al.* 1997). For simplicity however, we suppose here that the velocity fluctuations remain small and neglect M_l.

The advective term A_l is due to the relative motion of the interface in a reacting porous medium. It appears for instance during solidification, where it is related to the volume change (i.e. to the difference between ρ_l and ρ_s), which we neglect in the following.

The interfacial viscous stress exchange I_l corresponds to the microscopic momentum exchange of the Newtonian fluid with the solid matrix and must be related to the viscosity of the fluid, to the relative velocity of the solid and the liquid and to the morphology of the porous matrix. As a first approximation, this term can thus be written (Ochoa-Tapia & Whitaker 1995*a*)

$$I_l = -\eta[\boldsymbol{u}_l]f, \tag{2.9}$$

where f is some function of the morphology of the porous matrix. Since $I_l = 0$ in pure fluid,

$$f \to 0 \quad \text{when} \quad \chi \to 1. \tag{2.10}$$

For comparison with the standard Darcy's law, we will see in § 2.2 that it is convenient to write

$$I_l = -\frac{\eta\chi}{\Pi(\chi)}\boldsymbol{u}, \tag{2.11}$$

where the function Π introduced here corresponds to the permeability defined in Darcy's law and $\boldsymbol{u}$ is the Darcy velocity, defined as the volume flow rate per unit cross-sectional area. Hence with our notation,

$$\boldsymbol{u} = [\boldsymbol{u}_l] = \chi[\boldsymbol{u}_l]^l. \tag{2.12}$$

If we further suppose a mesoscopically incompressible fluid (i.e. $\nabla\cdot\boldsymbol{u} = 0$), and if we apply the Boussinesq approximation, the momentum equation finally becomes

$$\rho_l\frac{\partial}{\partial t}\boldsymbol{u} + \rho_l\boldsymbol{u}\cdot\nabla\left(\frac{\boldsymbol{u}}{\chi}\right) = -\chi\nabla[P_l]^l + \eta\nabla^2\boldsymbol{u} + \chi\rho_l\boldsymbol{g} - \frac{\eta\chi}{\Pi(\chi)}\boldsymbol{u}, \tag{2.13}$$

which is the Darcy–Brinkman equation. Using this equation implies that all fields χ, $[P_l]^l$, $\boldsymbol{u}$ and $\nabla\boldsymbol{u}$ are continuous through the whole domain. Although the general form of this equation is well known, variations of it can be found in the literature, especially in the location of the porosity within each term (e.g. Bennon & Incropera 1987; Shyy *et al.* 1997; Beckermann *et al.* 1999; Kaempfer & Rappaz 2003). Special care should be taken, since having the porosity inside or outside the gradients in (2.13) can lead to large effects when the porosity changes spatially, as for instance in a mushy layer.

2.2. *Limits of the Darcy–Brinkman equation*

We can non-dimensionalize (2.13) using a given velocity scale V and a given length scale L. If we choose the viscous pressure scale $P = \eta V/L$, then

$$Re\left[\frac{\partial}{\partial t}\boldsymbol{u} + \boldsymbol{u}\cdot\nabla\left(\frac{\boldsymbol{u}}{\chi}\right)\right] = -\chi\nabla[P_l]^l + \nabla^2\boldsymbol{u} - \chi\frac{\rho_l g L^2}{\eta V}\boldsymbol{e}_z - \chi\frac{L^2}{\Pi(\chi)}\boldsymbol{u}, \tag{2.14}$$

where $\boldsymbol{e}_z$ is a unit vertical vector and $Re = \rho_l V L/\eta$ the Reynolds number. In the pure-fluid limit, $\chi = 1$ and, from (2.10), $\Pi \to \infty$, so the Darcy–Brinkman equation gives the standard Navier–Stokes equation

$$Re\left(\frac{\partial}{\partial t}\boldsymbol{u} + \boldsymbol{u}\cdot\nabla\boldsymbol{u}\right) = -\nabla P + \nabla^2\boldsymbol{u} - \frac{\rho_l g L^2}{\eta V}\boldsymbol{e}_z, \tag{2.15}$$

where P is the liquid pressure.

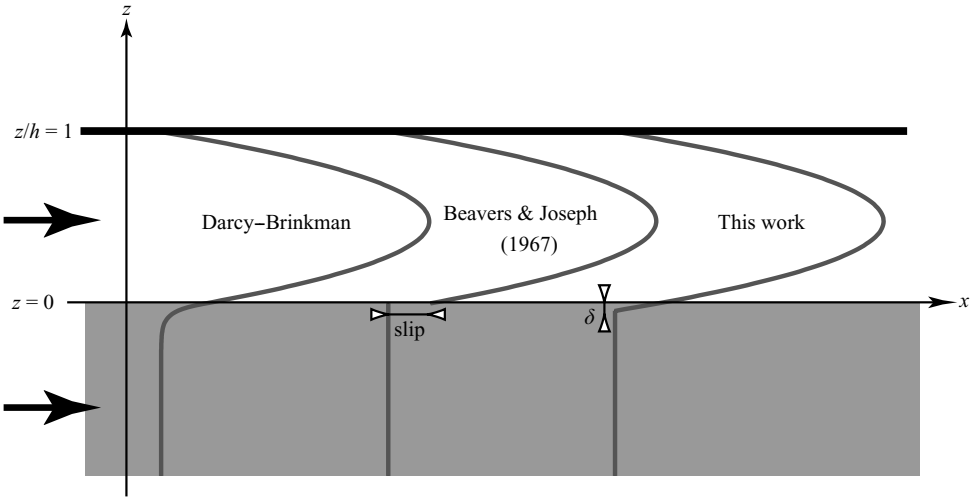

FIGURE 1. Poiseuille flow in a fluid overlying a porous layer: velocity profiles using the limiting Darcy–Brinkman formulation and Stokes–Darcy formulation with either Beavers & Joseph's (1967) interfacial conditions or the interfacial conditions proposed here. $\chi_f = 0.5$, $\Pi(\chi_f)/h^2 = 10^{-3}$ and $\eta^{-1}\mathrm{d}p/\mathrm{d}x = -1\,\mathrm{m}^{-1}\mathrm{s}^{-1}$.

If we instead choose Darcy's pressure scale $P = \eta LV/\Pi_0$ (where Π_0 is a characteristic scale of permability), we obtain

$$Da\ Re\left[\frac{\partial}{\partial t}\boldsymbol{u} + \boldsymbol{u}\cdot\nabla\left(\frac{\boldsymbol{u}}{\chi}\right)\right] = -\chi\left[\nabla[P_l]^l + \frac{\rho_l g \Pi_0}{\eta V}\boldsymbol{e}_z + \frac{\Pi_0}{\Pi(\chi)}\boldsymbol{u}\right] + Da\nabla^2\boldsymbol{u}, \qquad (2.16)$$

where $Da = \Pi_0/L^2$ is the Darcy number. In the limit $Da \to 0$, the Darcy–Brinkman equation gives the standard Darcy equation

$$\boldsymbol{u} = -\frac{\Pi(\chi)}{\Pi_0}\left(\nabla[P_l]^l + \frac{\rho_l g \Pi_0}{\eta V}\boldsymbol{e}_z\right). \qquad (2.17)$$

In the following, we study various flows in multiphase domains using both a single-domain approach, where we solve the Darcy–Brinkman equation through the whole domain, and a multiple-domain approach, where we solve Stokes' equation in the pure fluid and Darcy's equation in the porous matrix, with relevant interfacial conditions.

3. Poiseuille flow in a fluid overlying a porous layer

Following Beavers & Joseph (1967), we consider a two-dimensional Poiseuille flow in a channel formed by an impermeable wall at $z = +h$ and a permeable wall at $z = 0$ (cf. figure 1). The boundary at $z = 0$ corresponds to the upper surface of a semi-infinite porous medium with a fixed porosity χ_f and permeability $\Pi(\chi_f)$, saturated with the same fluid. A constant horizontal pressure gradient $\mathrm{d}p/\mathrm{d}x < 0$ is imposed through both the liquid and the porous medium, and we look for a velocity in the form $\boldsymbol{u} = (u(z), 0)$.

3.1. *Darcy–Brinkman formulation*

We first suppose that the fluid in the channel and in the porous medium follows the Darcy–Brinkman equation (2.13). Hence, defining the intrinsic volume average of the

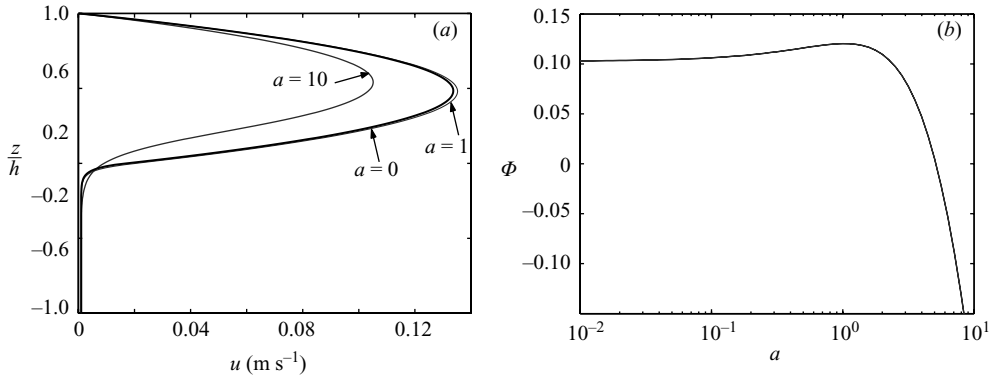

FIGURE 2. (*a*): Poiseuille flow profiles computed with Darcy–Brinkman formulation for various values of the averaging size $\delta_a = a\sqrt{\Pi(\chi_f)}$. (*b*): relative flow rate increase depending on the scaling coefficient a. In these computations, $\chi_f = 0.9$, $\Pi(\chi_f)/h^2 = 10^{-3}$ and $\eta^{-1}\mathrm{d}p/\mathrm{d}x = -1\,\mathrm{m}^{-1}\,\mathrm{s}^{-1}$.

dynamic pressure in the liquid as $p = [P_l]^l - \rho_l g z$, we have

$$0 = -\chi\frac{\mathrm{d}p}{\mathrm{d}x} + \eta\frac{\mathrm{d}^2u}{\mathrm{d}z^2} - \frac{\eta\chi}{\Pi(\chi)}u. \tag{3.1}$$

In the Darcy–Brinkman formulation, all fields correspond to average values over a mesoscopic volume and are continuous. To better illustrate this point, we suppose the mesoscopic averaging volume to be a cube with side length δ_a, typically a few pore lengths. Hence,

$$\delta_a = a\sqrt{\Pi(\chi_f)}, \tag{3.2}$$

where $a = O(1)$. Then, the liquid fraction is given by $\chi = \chi_f$ for $z \leqslant -\delta_a$, $\chi = 1.0$ for $z \geqslant +\delta_a$, and $\chi = (1-\chi_f)z/2\delta_a + (1+\chi_f)/2$ for $-\delta_a \leqslant z \leqslant \delta_a$. For a given permeability function following condition (2.10), (3.1) can be solved with the boundary conditions

$$u(h) = 0 \quad \text{and} \quad \frac{\mathrm{d}u}{\mathrm{d}z}(-\infty) = 0. \tag{3.3}$$

For instance, computed profiles are shown in figure 2(*a*), using the Carman–Kozeny permeability function (Bear 1972)

$$\Pi(\chi) = \Pi_0\frac{\chi^3}{(1-\chi)^2}, \tag{3.4}$$

where Π_0 is a reference permeability.

Computed results depend both on the choice of the permeability function and on the choice of the averaging length δ_a. However, in all cases the solution converges towards a single limit when $\delta_a \to 0$ (figure 2*b*), which only depends on the permeability and the porosity of the porous domain. This limit can be determined analytically by solving

$$0 = -\frac{\mathrm{d}p}{\mathrm{d}x} + \eta\frac{\mathrm{d}^2u}{\mathrm{d}z^2} \quad \text{in the liquid} \quad (0 < z \leqslant h), \tag{3.5a}$$

$$0 = -\chi_f\frac{\mathrm{d}p}{\mathrm{d}x} + \eta\frac{\mathrm{d}^2u}{\mathrm{d}z^2} - \frac{\eta\chi_f}{\Pi(\chi_f)}u \quad \text{in the porous matrix} \quad (-\infty < z < 0). \tag{3.5b}$$

Hence, with $u(h) = 0$ and u finite as $z \to -\infty$,

$$u(z) = \frac{1}{2\eta}\frac{\mathrm{d}p}{\mathrm{d}x}(z-h)(z-A) \quad \text{in the liquid,} \tag{3.6a}$$

$$u = B\mathrm{e}^{z/\delta} - \frac{\chi_f \delta^2}{\eta}\frac{\mathrm{d}p}{\mathrm{d}x} \quad \text{in the porous matrix,} \tag{3.6b}$$

where A and B are constants to be determined and

$$\delta = \sqrt{\frac{\Pi(\chi_f)}{\chi_f}}. \tag{3.7}$$

Since we use a continuous formulation through both the liquid and the porous matrix, the velocity u as well as its derivative $\mathrm{d}u/\mathrm{d}z$ must be continuous at $z = 0$. This leads to

$$A = -\frac{h\delta + 2\chi_f\delta^2}{h+\delta}, \quad B = -\frac{\delta}{2\eta}\frac{\mathrm{d}p}{\mathrm{d}x}\frac{h^2 - 2\chi_f\delta^2}{h+\delta}. \tag{3.8}$$

The length scale of the transition zone δ and the averaging length δ_a are of the same order of magnitude. Hence, the limit solution $\delta_a = 0$ with $\delta \neq 0$ is not mathematically rigorous. Nevertheless, we use it in the following since it is analytically tractable and since it correctly illustrates the behaviour of the full solution (see Ochoa-Tapia & Whitaker (1995*b*) for a complete and mathematically rigorous treatment of this configuration).

3.2. *Comparison with Beavers & Joseph (1967)*

Following Beavers & Joseph (1967), we then compute the relative increase in flow rate due to the porous wall

$$\Phi = \left[-\frac{1}{12\eta}\frac{\mathrm{d}p}{\mathrm{d}x}h^3\right]^{-1}\int_0^h u(z)\,\mathrm{d}z - 1, \tag{3.9}$$

(plotted in figure 2*b* for general values of a), where the denominator corresponds to the flow rate for an impermeable lower wall or for a vanishing tangential velocity at the interface, corresponding to (3.6*a*) with $A = 0$. In order to compare with Beavers & Joseph (1967), we define

$$\alpha = \sqrt{\chi_f} \quad \text{and} \quad \sigma = \frac{h}{\sqrt{\Pi(\chi_f)}}, \tag{3.10}$$

where σ is the inverse of the square root of the Darcy number. Then, the relative flow rate increase for the limiting case of Darcy–Brinkman is

$$\Phi = \frac{3(\sigma + 2\alpha)}{\sigma(1+\alpha\sigma)}. \tag{3.11}$$

This is exactly the relationship found by Beavers & Joseph (1967), using Stokes' equation in the liquid, Darcy's equation in the porous matrix, and their slip boundary condition at the interface (1.1). Compared to their results, we now have a physical interpretation of the coefficient α for the limiting Darcy–Brinkman case, where α is equal to the square root of the porosity. This agrees with Beavers & Joseph's (1967) conclusion that the coefficient α depends particularly on structural parameters characterizing the nature of the porous surface rather than on the viscosity of the fluid or on the permeability itself.

Taking (3.10), the Darcy–Brinkman velocity and the Beavers & Joseph (1967) velocity in the pure fluid and deep in the porous matrix are exactly equal. There

are differences only in the viscous transition zone, where the exponential decay in the Darcy–Brinkman formulation is replaced by a sharp jump in Beavers & Joseph (1967).

3.3. *New interfacial conditions between Stokes and Darcy solutions*

In our notation, the Beavers & Joseph (1967) interface condition (1.1) can be written

$$u_D = u_S(0) - \delta \frac{\mathrm{d}u_S}{\mathrm{d}z} = u_S(-\delta). \tag{3.12}$$

This can be interpreted as that, in the mixed Stokes–Darcy approach, the Stokes velocity is extrapolated up to a depth $-\delta$, where it is continuous with the Darcy velocity. Indeed, Darcy's law is a volume-averaged relationship in the porous matrix, and it cannot be defined on scales smaller than the averaging length δ_a: in particular, Darcy's law is not valid at a distance closer than δ_a to the interface, and any boundary condition between Stokes and Darcy formulation must be formulated deeper than this.

This conclusion can also be seen in the force balance suggested by the Darcy–Brinkman equation. In the liquid, the pressure gradient is balanced by fluid–fluid interactions (i.e. Stokes' equation). Deep in the porous medium, the pressure gradient is balanced by viscous dissipation against the solid matrix (i.e. Darcy's equation). Just below the interface, a transition zone exists in which both physical interactions are present. A simple estimation of the forces indicates that Darcy's term becomes larger than the fluid–fluid interaction once

$$\eta \nabla^2 u \sim \eta \frac{u}{z^2} < \frac{\eta \chi_f}{\Pi(\chi_f)} u, \tag{3.13}$$

which means

$$z < -\sqrt{\frac{\Pi(\chi_f)}{\chi_f}} = -\delta. \tag{3.14}$$

Hence, to leading order, Stokes' equation remains valid up to the depth $-\delta$.

In any multiphase-flow study using the mixed Stokes–Darcy formulation, we therefore suggest a generalized interface condition corresponding to continuity of the velocity vector (as well as of the liquid pressure) at the position $z_i - \delta$, where z_i is the porous matrix–liquid interface position and δ is the characteristic size of the viscous transition zone (a few pore lengths):

$$\boldsymbol{u}_S(z_i - \delta) = \boldsymbol{u}_D(z_i - \delta) \quad \text{with} \quad \delta = c\sqrt{\frac{\Pi(\chi_f)}{\chi_f}}, \tag{3.15}$$

where c is a constant of order 1 ($c = 1$ for the limiting Darcy–Brinkman case).

This new interfacial condition appears to be very close to Beavers & Joseph's (1967) suggestion, and it also necessitates an unknown constant. Nevertheless, it is both physically justified and simpler to implement, especially in numerical simulations. Besides, this new interfacial condition leads to a relative flow rate increase in the Poiseuille geometry of

$$\Phi = \frac{3(\sigma + 2\alpha + 1/\alpha)}{\sigma(1 + \alpha\sigma)}, \tag{3.16}$$

where $\alpha = \sqrt{\chi_f}/c$. As illustrated in figure 3, this equation leads to a slightly better agreement with the experiments of Beavers & Joseph (1967). We thus expect these interfacial conditions to be more accurate.

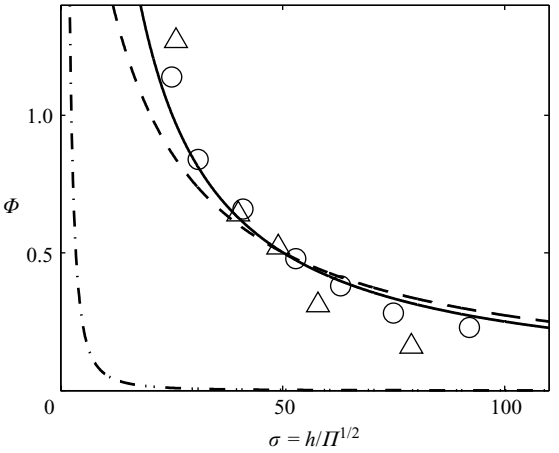

FIGURE 3. Relative flow rate increase as a function of the inverse of the square root of the Darcy number. Triangles and circles represent experimental measurements by Beavers & Joseph (1967) using aloxite porous specimens. The continuous line corresponds to the best fit according to (3.16) ($\alpha = 0.12$), using our proposed interfacial conditions (3.15). The dashed line corresponds to the best fit according to (3.11) ($\alpha = 0.1$), using Beavers & Joseph's (1967) interfacial conditions (1.1) or the limiting Darcy–Brinkman formulation (see § 3.1). The dashed-dotted line corresponds to a continuous velocity at the interface, given by the limit of (3.16) when $\delta \to 0$, i.e. when $\alpha \to \infty$. By definition, the condition of zero tangential velocity leads to $\Phi = 0$.

We will now test and compare these various formulations in a corner flow, where a vertical flux through the interface also takes place and leads to larger variations.

4. Corner flow in a fluid overlying a porous layer

We consider a corner flow in a domain $0 \leqslant z \leqslant h$, $0 \leqslant x < \infty$, with pure fluid in the upper half $h/2 < z \leqslant h$ and a porous matrix of porosity χ and permeability $\Pi(\chi)$, saturated with the same fluid, in the lower half $0 \leqslant z < h/2$ (figure 4). At $z = h$, a purely vertical input velocity $\boldsymbol{u} = (0, -V)$ is imposed; at the lower wall $z = 0$, we suppose no vertical velocity $v = 0$ and no horizontal shear $\partial u/\partial z = 0$; at the vertical wall $x = 0$, we suppose no horizontal velocity $u = 0$ and no vertical shear $\partial v/\partial x = 0$. We look for the stationary solution and we suppose that the flow is sufficiently slow to neglect inertial effects (i.e. the left-hand side of (2.13) is zero).

Following the well-known results in the case of a pure fluid (e.g. Batchelor 1967), we look for a solution of the form

$$\boldsymbol{u} = (-xVf'(z), Vf(z)), \tag{4.1}$$

which directly satisfies the mass conservation equation ($\nabla \cdot \boldsymbol{u} = 0$) and the boundary conditions at the vertical wall. We thus look for a function f that satisfies the equations of motion as well as the boundary conditions

$$f(h) = -1, \quad f'(h) = 0, \quad f(0) = 0 \quad \text{and} \quad f''(0) = 0. \tag{4.2}$$

In the following, all equations are non-dimensionalized using the input velocity V, the depth of the domain h and the viscous pressure scale $\eta V/L$.

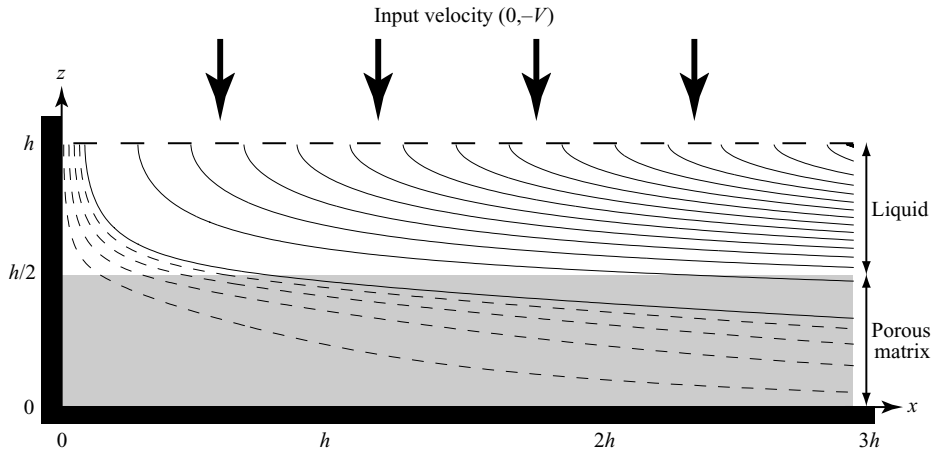

FIGURE 4. Corner flow in a fluid overlying a porous layer with a constant porosity: geometry and streamlines given by the limiting Darcy–Brinkman solution with constant $\chi_f = 0.2$ and $Da = 10^{-3}$. Continuous streamlines are equally spaced from 0.1 to 2.9 with a spacing 0.2, and dashed streamlines from 0.02 to 0.08 with a spacing 0.02.

4.1. *Constant porosity*

We first consider that the porous matrix has a constant porosity χ_f and a constant permeability $\Pi(\chi_f)$.

4.1.1. *Darcy–Brinkman formulation*

For $0 \leqslant z \leqslant 1$, the fluid follows the Darcy–Brinkman equation

$$0 = -\nabla p + \frac{1}{\chi}\nabla^2 \boldsymbol{u} - \frac{h^2}{\Pi(\chi)}\boldsymbol{u}. \tag{4.3}$$

Using (4.1) and eliminating the pressure, we find

$$0 = \frac{\mathrm{d}}{\mathrm{d}z}\left[\frac{1}{\chi}f''' - \frac{h^2}{\Pi(\chi)}f'\right]. \tag{4.4}$$

As previously, this equation can be solved for any given averaging size δ_a and permeability function. All solutions converge towards a single limit when $\delta_a \to 0$. Taking into account (4.4) and the fact that $\chi \to 1$ and $\Pi(\chi) \to \infty$ in the liquid, $\chi \to \chi_f$ and $\Pi(\chi) \to \Pi(\chi_f)$ in the porous matrix, the limiting solution can be found analytically by solving

$$0 = f^{\mathrm{iv}} \quad \text{in the liquid} \quad (1/2 < z \leqslant 1), \tag{4.5a}$$

$$0 = f^{\mathrm{iv}} - \frac{1}{\delta^2}f'' \quad \text{in the porous matrix} \quad (0 \leqslant z < 1/2), \tag{4.5b}$$

where

$$\delta = \sqrt{\frac{Da}{\chi_f}} \quad \text{and} \quad Da = \frac{\Pi(\chi_f)}{h^2}. \tag{4.6}$$

Hence, taking (4.2) into account,

$$f(z) = -1 + A(z-1)^2 + B(z-1)^3 \quad \text{in the liquid}, \tag{4.7a}$$

$$f(z) = C\,\sinh(z/\delta) + Dz \quad \text{in the porous matrix}, \tag{4.7b}$$

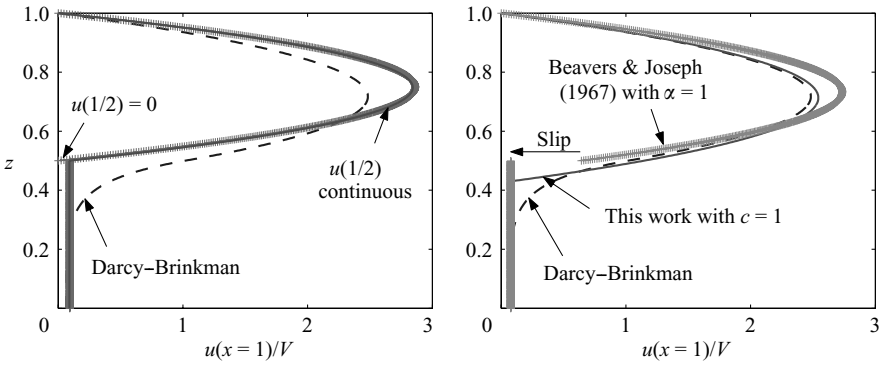

FIGURE 5. Horizontal velocity profiles with $\chi_f = 0.2$, $Da = 10^{-3}$, for the various proposed interface boundary conditions.

where the constants A–D are determined from the interfacial conditions that f and its first two derivatives must be continuous. Additionally, continuity of pressure at the interface requires that

$$f'''|_{(1/2)^+} = \frac{1}{\chi_f} f''' - \frac{1}{Da} f'|_{(1/2)^-}. \tag{4.8}$$

The solution can be found straightforwardly and is plotted as a dashed curve in figure 5.

4.1.2. *Mixed Stokes–Darcy formulation*

In the pure liquid domain, the velocity again obeys the Stokes equation (4.5*a*), and the function f_S is given by (4.7*a*). However, in the porous matrix, the velocity follows Darcy's equation

$$0 = -\nabla p - \frac{1}{Da}\boldsymbol{u}, \tag{4.9}$$

which gives

$$f_D'' = 0 \quad \text{with} \quad f_D(0) = 0 \quad \Rightarrow \quad f_D(z) = Cz. \tag{4.10}$$

The constants A–C are determined by three interfacial conditions between the Stokes and Darcy regions. In all cases, continuity of pressure requires that

$$-f_S''' = \frac{1}{Da} f_D'. \tag{4.11}$$

The two addtional constraints depend on the chosen interfacial conditions. For our interfacial conditions (3.15), we introduce the typical size of the viscous transition δ as

$$\delta = c\sqrt{\frac{Da}{\chi_f}}, \tag{4.12}$$

where c is a scaling constant, and write the continuity of the velocity vector at $z_\delta = 1/2 - \delta$:

$$-1 + A(z_\delta - 1)^2 + B(z_\delta - 1)^3 = Cz_\delta \quad \text{and} \quad 2A(z_\delta - 1) + 3B(z_\delta - 1)^2 = C. \tag{4.13}$$

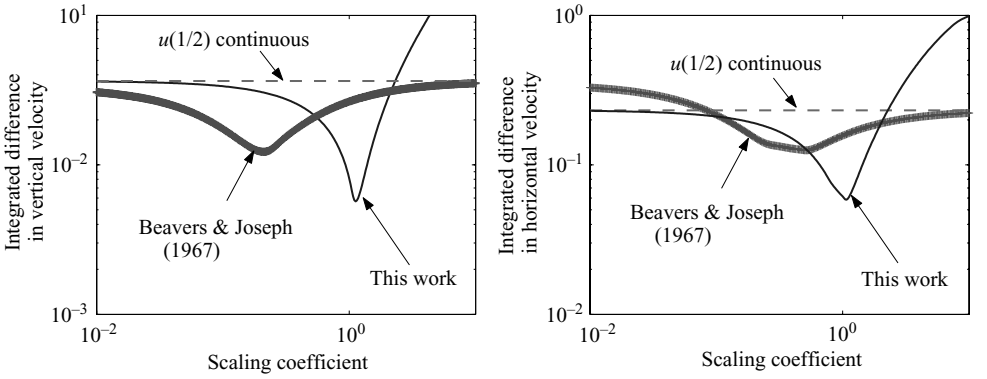

FIGURE 6. Integrated difference between the mixed Stokes–Darcy and Darcy–Brinkman results as a function of the scaling coefficient (i.e. α for Beavers & Joseph (1967) and c for our interfacial conditions) for a corner flow in a fluid overlying a porous layer with a constant porosity ($Da = 10^{-3}$ and $\chi_f = 0.2$).

For Beavers & Joseph's (1967) conditions, the continuity in normal velocity and the slip condition (1.1) at $z = 1/2$ imply that

$$-1 + A/4 - B/8 = C/2 \quad \text{and} \quad -A + 3B/4 - C = \frac{\sqrt{Da}}{\alpha}(2A - 3B), \tag{4.14}$$

where α is a constant to be determined.

4.1.3. *Results*

Horizontal velocity profiles for the limiting Darcy–Brinkman formulation as well as for the Stokes–Darcy formulation with various suggested interfacial conditions are presented in figure 5. We also depict in figure 6 the integrated difference between a given formulation and the Darcy–Brinkman results, for both the vertical and the horizontal velocities.

Both conditions of continuous horizontal velocity at $z = 1/2$ and zero horizontal velocity at $z = 1/2$ are incompatible with the Darcy–Brinkman results: they lead to differences of several percent throughout the whole liquid region. Beavers & Joseph's (1967) interfacial conditions and our interfacial conditions can be adapted through their respective scaling coefficient, and give a small difference confined to the neighbourhood of the interface only. The best correspondence for both the vertical and the horizontal velocities is obtained with our boundary conditions for $c \sim 1$. The dependence on Darcy number Da is shown in figure 7 for both a continuous tangential velocity at $z = 1/2$ and our interfacial conditions. In all cases, the difference between the Darcy–Brinkman and Stokes–Darcy formulation decreases with the Darcy number, and all formulations are formally consistent in the limit $Da \to 0$: the flow then focuses into the fluid part of the system only, with zero velocity in the porous medium. Note however that at $Da = 10^{-6}$ the relative difference is two orders of magnitude smaller when using our interfacial condition than using continuity of the velocity at $z = 1/2$.

In figure 8, we show the relative flow rate increase in the pure fluid, compared to the classical interfacial condition of zero tangential velocity. Unlike for the Poiseuille geometry (see § 3.2), the Darcy–Brinkman method and Beavers & Joseph's (1967) interfacial conditions do not give the same results. Rather, two opposite trends take place: Darcy–Brinkman and our interfacial conditions suggest a possible decrease of

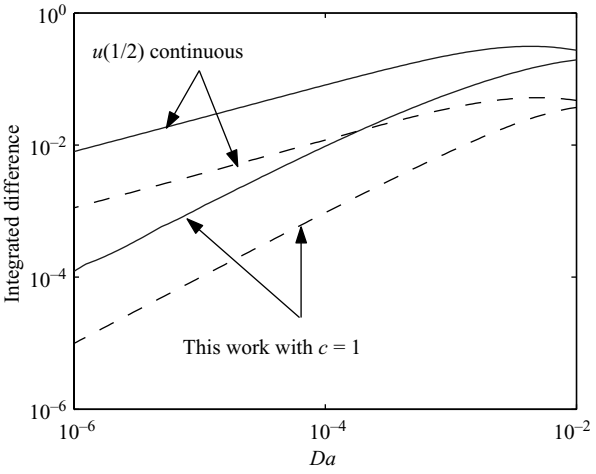

FIGURE 7. Integrated difference in horizontal (continuous line) and vertical (dashed line) velocities between mixed the Stokes–Darcy and Darcy–Brinkman results as a function of the Darcy number for $\chi_f = 0.2$, using our interfacial condition with $c = 1$ or a continuous horizontal velocity at $z = 1/2$.

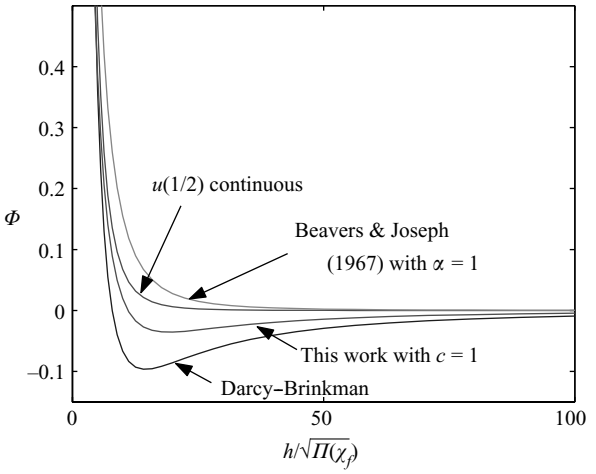

FIGURE 8. Relative flow rate increase as a function of the inverse of the square root of the Darcy number with $\chi_f = 0.2$, for the various proposed interfacial boundary conditions. By definition, the condition of zero tangential velocity leads to $\Phi = 0$.

the flow rate, whereas Beavers & Joseph's (1967) interfacial condition and continuity of the velocity always show $\Phi > 0$. This suggests an experimental test that could be used to differentiate between these various formulations.

4.2. *Linear porosity*

The previous simple example was solved analytically, so the jump in porosity could be accommodated when solving the Darcy–Brinkman equation. However, the Darcy–Brinkman formulation is most often used in numerical studies of systems in which the porosity exhibits large-scale variations and continuous transition towards the pure fluid (e.g. mushy layers). To investigate the consequences of this, we now consider

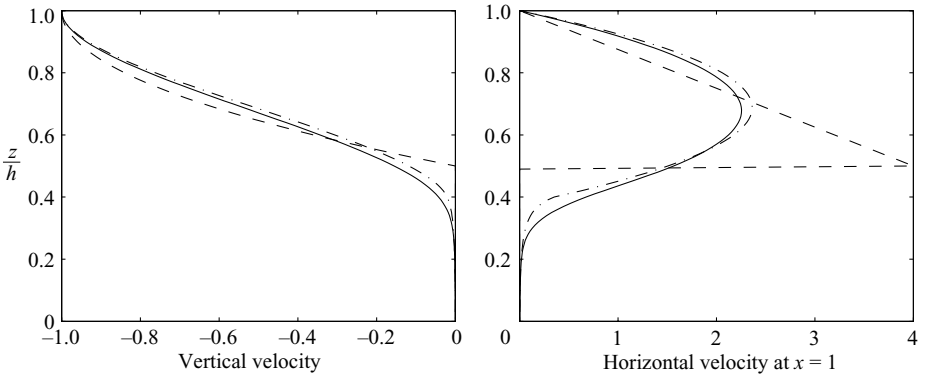

FIGURE 9. Comparison between the mixed Stokes–Darcy and Darcy–Brinkman formulations for a corner flow in a fluid overlying a porous layer with a linear porosity ($Da = 10^{-4}$ and $\chi_0 = 0.5$). Continuous line: Darcy–Brinkman; dashed line: mixed Stokes–Darcy in the limit $z_\delta \to (1/2)^-$ (i.e. $c \to 0$); dashed-dotted line: mixed Stokes–Darcy with $c = 1$.

the same configuration but with a porosity changing linearly from 1 at the interface $z = 1/2$ to χ_0 at $z = 0$, i.e.

$$\chi(z) = \chi_0 + 2(1 - \chi_0)z. \tag{4.15}$$

4.2.1. *Darcy–Brinkman formulation*

For $0 \leqslant z \leqslant 1$, the fluid follows the Darcy–Brinkman equation (4.4), with the porosity given by (4.15) and the Carman–Kozeny relationship (3.4). We solved this ordinary differential equation numerically, subject to the boundary conditions (4.2). Results are shown in figure 9.

4.2.2. *Mixed Stokes–Darcy formulation*

In the pure liquid domain, the function f_S is again given by (4.7*a*). In the porous matrix, the velocity follows Darcy's equation. Eliminating the pressure, one finds

$$\frac{\mathrm{d}}{\mathrm{d}z}\left[\frac{f_D'(z)}{\Pi(\chi)}\right] = 0, \tag{4.16}$$

which, using the porosity given by (4.15), the Carman–Kozeny relationship (3.4), and taking into account that $f_D(0) = 0$, can be solved to give

$$f_D(z) = f_D'(0)\frac{1 - \chi_0}{2\chi_0^3}G(z), \tag{4.17}$$

where

$$G(z) = \frac{1}{1 - \chi_0}\frac{2z}{1 - 2z} + 3\ln(1 - 2z) + 6(1 - \chi_0)z + 2(1 - \chi_0)^2 z(z - 1). \tag{4.18}$$

The three unknown constants A, B and $f'(0)$ are determined by the interfacial conditions. When using the Carman–Kozeny permeability function, $\Pi \to \infty$ when $z \to 1/2$. Hence, physically, Darcy's equation is not relevant near the interface $z = 1/2$. Moreover, mathematically, no interfacial conditions between the Stokes and Darcy domains taken at $z = 1/2$ are usable. We can however use our interfacial conditions, which lead to f, f' and the pressure all being continuous at a depth $z_\delta = 1/2 - \delta$.

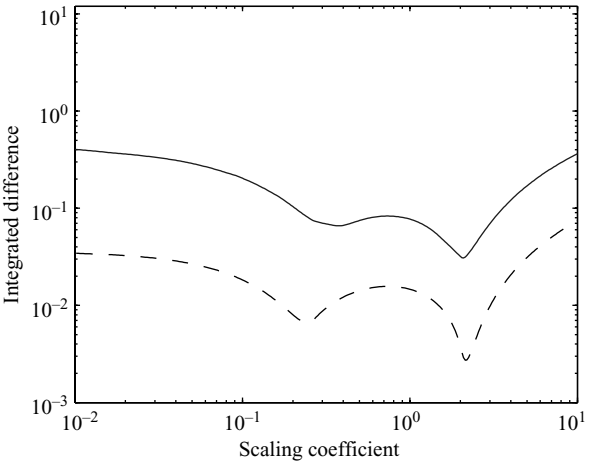

FIGURE 10. Integrated difference in horizontal (continuous line) and vertical (dashed line) velocities between the mixed Stokes–Darcy and Darcy–Brinkman results as a function of the scaling coefficient c for a corner flow in a fluid overlying a porous layer with a linear porosity ($Da = 10^{-4}$ and $\chi_0 = 0.5$).

The latter implies

$$-f_S'''(z_\delta) = \frac{1}{Da}\frac{(1-\chi_\delta)^2}{\chi_\delta^3} f_D'(z_\delta), \tag{4.19}$$

where now $Da = \Pi_0/h^2$.

The definition of δ is not as straightforward as in the case of constant porosity, since the porosity and the permeability change with depth. We suggest calculating δ using (3.15) with the local value of the porosity and the permeability, i.e. non-dimensionally

$$\delta = c\sqrt{\frac{\Pi(z_i-\delta)/h^2}{\chi(z_i-\delta)}}, \tag{4.20}$$

where c is a scaling constant. With a linear porosity and Carman–Kozeny permeability, this is a polynomial equation in δ. In general, since we expect δ to be small and $\chi(z_i-\delta)$ to be very close to 1, a first-order development of (4.20) using (3.4) gives

$$\delta = \sqrt{\frac{c}{\chi'(z_i)}} Da^{1/4}. \tag{4.21}$$

4.2.3. *Results*

Typical profiles for Darcy–Brinkman and mixed Stokes–Darcy formulations are presented in figure 9. The integrated difference between the two formulations is shown as a function of the scaling coefficient c in figure 10. In the present case, continuity of velocity at the fluid–porous matrix interface ($c \to 0$) gives unrealistic results, where the horizontal velocity is maximum at the interface with a sharp jump between the two domains. This behaviour is mainly due to the divergence of the permeability given by the Carman–Kozeny equation when the liquid fraction goes to 1. In contrast, the Darcy–Brinkman formulation and our interfacial conditions smooth this discontinuity by introducing a viscous transition layer between the liquid and the porous matrix. Note that $\delta \sim Da^{1/4}$ now rather than $\delta \sim Da^{1/2}$ for constant porosity. Hence, the effects of the viscous layer remain important over a large depth,

even for very small Darcy number. The best agreement between the two formulations is obtained for $c \sim 2$.

This simple example illustrates how the choice of the interfacial condition influences the macroscopic computed results. As we will now see, this will be especially important when studying the solidification of a binary alloy, since first-order results regarding macroscopic physical properties (especially the bulk concentration) will depend strongly on the chosen velocity conditions at the interface.

5. Directional solidification in a corner flow

Our interest in comparing the single-domain Darcy–Brinkman model with the multiple-domain Stokes–Darcy model for flows through adjacent porous and pure-fluid domains stems from modelling interactions between flow and solidification within mushy layers. We therefore conclude by examining a simple problem of alloy solidification, where some of these issues can be confronted.

5.1. *Simplified physical model*

We consider a binary alloy in the corner-flow geometry with the boundary conditions introduced in the previous section, and we further suppose that the incoming fluid at $z = h$ has a fixed temperature T_∞ and a fixed concentration C_∞, while the temperature of the lower boundary at $z = 0$ is fixed just above the eutectic temperature T_e. A mushy layer then grows from this lower boundary, leading to a time-evolving porosity field. Following classical studies on solidification, we suppose that the whole system is pulled vertically at a constant rate V_{pull} and we look for a stationary solution in the moving frame of reference.

The solidifying binary alloy is fully characterized by five independent variables: the average enthalpy h; the average species concentration C; the two-dimensional Darcy velocity vector $\boldsymbol{u}$; and the liquid fraction χ. These five variables are determined by five coupled equations characterizing the transport of enthalpy, species, mass and momentum, as well as the thermodynamic constraint imposed by the phase diagram. Three other useful variables can be derived from these primary unknowns, i.e. the temperature T, the liquid enthalpy h_l and the liquid concentration C_l.

We denote by k_k the thermal conductivity, $c_{p,k}$ the heat capacity per unit volume and D_k the species diffusivity of the liquid ($k = l$) and the solid ($k = s$) respectively. To keep the problem simple, we make the following assumptions. We neglect variations of material properties inside the control volume ΔV, and suppose that the solid and the liquid have the same physical properties, i.e. $[\rho_l]^l = [\rho_s]^s = \rho$, $[k_l]^l = [k_s]^s = k$, and $[c_{p,l}]^l = [c_{p,s}]^s = c_p$. We neglect species diffusion, i.e. $[D_l]^l = [D_s]^s = 0$. We suppose that the temperature is constant inside the control volume ΔV, i.e. $[T_l]^l = [T_s]^s = T$, and that the liquid is well mixed inside the control volume ΔV, i.e. $[C_l]^l = C_l$. Also, we consider a simplified equilibrium phase diagram, where the solidus and liquidus curves are respectively given by

$$C = 0 \quad \text{or} \quad T_{solidus}(C) = T_e, \tag{5.1a}$$

$$T_{liquidus}(C) = T_m - \frac{T_m - T_e}{C_e} C, \tag{5.1b}$$

where C_e corresponds to the eutectic concentration and T_m to the liquidus temperature at $C = 0$.

In the corner-flow geometry, we look for a solution in which the enthalpy, temperature, concentrations, liquid fraction, and velocity function f depend on time

t and depth z only. We define the dimensionless temperature and concentration by

$$\theta = \frac{T - T_e}{T_\infty - T_e}, \quad C = \frac{C - C_e}{C_\infty - C_e} \tag{5.2}$$

and introduce the following characteristic scales: energy $c_p(T_\infty - T_e)$; length h; time h^2/κ, where $\kappa = k/c_p$; velocity κ/h; pressure $\eta\kappa/h^2$. Then, the dimensionless mesoscopic transport equations in the moving frame of reference, derived from their microscopic counterpart using the volume-averaging method (see for instance Beckermann & Viskanta 1988), are

$$\frac{\partial h}{\partial t} + (f - V_{pull})\frac{\partial h}{\partial z} - \frac{\partial^2 h}{\partial z^2} = Lf\frac{\partial \chi}{\partial z} - L\frac{\partial^2 \chi}{\partial z^2}, \tag{5.3}$$

$$\frac{\partial C}{\partial t} + \left(\frac{f}{\chi} - V_{pull}\right)\frac{\partial C}{\partial z} - \frac{1}{\chi^2} f \frac{\partial \chi}{\partial z} C = \frac{1}{\chi^2} f \frac{\partial \chi}{\partial z}\frac{C_e}{C_\infty - C_e}, \tag{5.4}$$

where

$$h_l = L + \theta, \quad h = \chi L + \theta, \tag{5.5}$$

and since we suppose here that the system remains strictly above the eutectic temperature,

$$C = \chi C_l + (\chi - 1)\frac{C_e}{C_\infty - C_e}. \tag{5.6}$$

To close the problem, finally we rewrite the relationships given by the phase diagram in terms of enthalpy. For any given (C, h), we compute

$$h_{liquidus}(C) = L + mC, \tag{5.7}$$

where m is the dimensionless liquidus slope

$$m = \frac{T_m - T_e}{T_\infty - T_e}\frac{C_\infty - C_e}{-C_e}. \tag{5.8}$$

Then, if $h \geqslant h_{liquidus}(C)$, $\chi = 1$; else, since we remain strictly above the eutectic, the temperature and liquid concentration are related by the liquidus

$$\theta = mC_l, \tag{5.9}$$

and from (5.5) and (5.6), χ is the solution between 0 and 1 of the second-order equation

$$h = \chi L + m\left[\frac{C}{\chi} + \left(\frac{1}{\chi} - 1\right)\frac{C_e}{C_\infty - C_e}\right]. \tag{5.10}$$

Note that using the enthalpy and bulk concentration instead of the temperature and liquid concentration in the transport equations prevents us from calculating $\partial\chi/\partial t$ directly: rather, χ is determined using the known values of h and C and the phase diagram.

5.2. *Solution strategy and numerical approach*

Our initial state at $t = 0$ is defined by $\theta = 1$ except that $\theta(0) = 0$, $C = 1$, and $\chi = 1$ except that $\chi(0) = 1 + (C_\infty - C_e)/C_e$, which comes from (5.6) with $C_l(0) = \theta(0)/m = 0$. Hence, $h = L + 1$ except that $h(0) = L(1 + (C_\infty - C_e)/C_e)$. We then progressively increment time until the steady state is reached. Knowing all fields at time t^n, we successively compute all fields at time $t^{n+1} = t^n + \Delta t$ in four successive steps. We

first compute h^{n+1} using a time-implicit space-centred discretization of (5.3) with the boundary conditions

$$h_{z=1}^{n+1} = L + 1 \quad \text{and} \quad h_{z=0}^{n+1} = \chi_{z=0}^{n} L. \tag{5.11}$$

We then compute C^{n+1} using a time-implicit space-upwind discretization of (5.4) with the boundary condition

$$C_{z=1}^{n+1} = 1. \tag{5.12}$$

From (C^{n+1}, h^{n+1}), we compute χ^{n+1} using the process described in (5.7)–(5.10).

Neglecting advective terms as well as convective terms (i.e. ρ_l does not depend on θ nor on C_l), we finally compute f^{n+1} using χ^{n+1} and either the Darcy–Brinkman equation (4.4) or the mixed Stokes–Darcy equations (4.7*a*) and (4.16). As in the previous section, since $\chi \to 1$ at the interface, only our interfacial conditions can be used with the Carman–Kozeny permeability. At each time step, we then compute z_δ^{n+1}, the interfacial position for velocity boundary conditions, using local values of porosity and permeability, i.e.

$$z_\delta^{n+1} = z_\chi^{n+1} - c\sqrt{\frac{\Pi^{n+1}(z_\delta^{n+1})/h^2}{\chi^{n+1}(z_\delta^{n+1})}}, \tag{5.13}$$

where c is a scaling constant and z_χ^{n+1} the position of the liquid–porous matrix interface. However, in order to compare with previous multiple-domain studies of solidification (e.g. Schulze & Worster 1999), we also present here results computed with either a continuous tangential velocity at z_χ^{n+1} or Beavers & Joseph's (1967) interfacial conditions at z_χ^{n+1}, using a non-divergent permeability function

$$\hat{\Pi} = \hat{\Pi}_0 \chi^3. \tag{5.14}$$

In these cases, $\hat{\Pi}_0$ is chosen such that $\Pi(z = 0) = \hat{\Pi}(z = 0)$.

5.3. *Results*

Typical steady-state profiles for the Darcy–Brinkman and mixed Stokes–Darcy formulations with our interfacial conditions are presented in figure 11. One can see that the steady-state porosity profile is close to linear. Hence, as previously, velocities given by the limit $c \to 0$ are unrealistic, whereas $c \sim 1$ gives qualitatively good agreement between single-domain and multiple-domain formulations. The simple case of solidification studied here demonstrates that the predicted macroscopic bulk concentration field is very sensitive to the choice of interfacial conditions: significant variations take place throughout the whole depth of the solid formed. This is mainly due to the assumption of no species diffusion: the bulk concentration is only advected, and thus highly sensitive to the velocity field. In most natural and industrial settings, the Lewis number (i.e. the ratio of thermal to species diffusivity) is large and this conclusion will remain valid. As shown in figure 12, the agreement between the two formulations can be adjusted through the choice of the scaling coefficient c. It is not possible to choose a value that gives simultaneously the best agreement for all macroscopic fields, but values of $c \sim$2–4 work reasonably well.

Steady-state profiles obtained with the mixed Stokes–Darcy formulation with a continuous tangential velocity or Beavers & Joseph's (1967) conditions at the liquid–porous interface are presented in figure 13. Significant differences in all macroscopic fields between these formulations and the Darcy–Brinkman formulation are observed through the whole depth of the system, which can be adjusted neither by the scaling coefficient α nor by the permeability function.

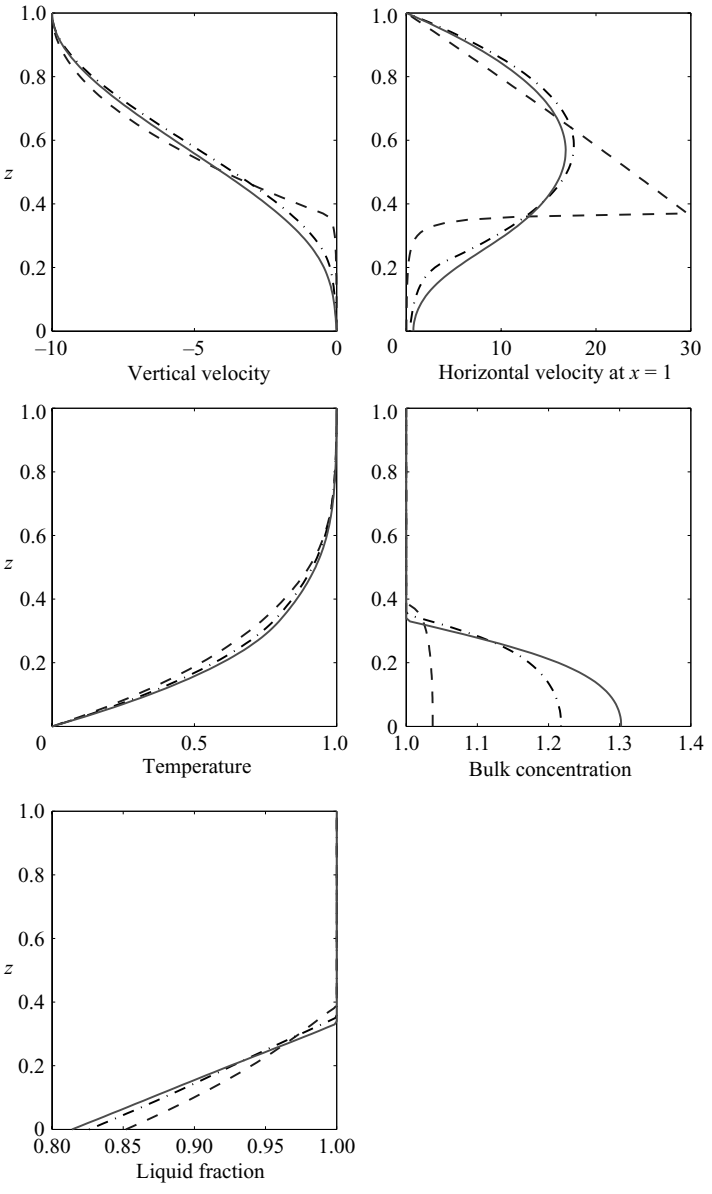

FIGURE 11. Comparison between steady-state profiles given by the Darcy–Brinkman formulation (continuous line) and the mixed Stokes–Darcy formulation with our interfacial conditions for the solidification of a binary alloy in a corner flow ($V_{pull} = 1$, $V = 10$, $L = 10$, $Da = 10^{-4}$, $C_e/(C_\infty - C_e) = -7$, $m = 0.8$). Dashed line: mixed Stokes–Darcy in the limit $c \to 0$; dashed-dotted line: mixed Stokes–Darcy with $c = 1$.

Special care should thus be taken in the choice of the microscopic fluid–porous matrix interface conditions when determining realistic macrosegregation patterns of binary alloy solidification in industrial or natural settings. Differences calculated here with a simplified physical model would be even larger when taking into account buoyancy effects, since then velocities and bulk concentration would actively interact. Direct comparison with experiments is necessary to validate a given approach.

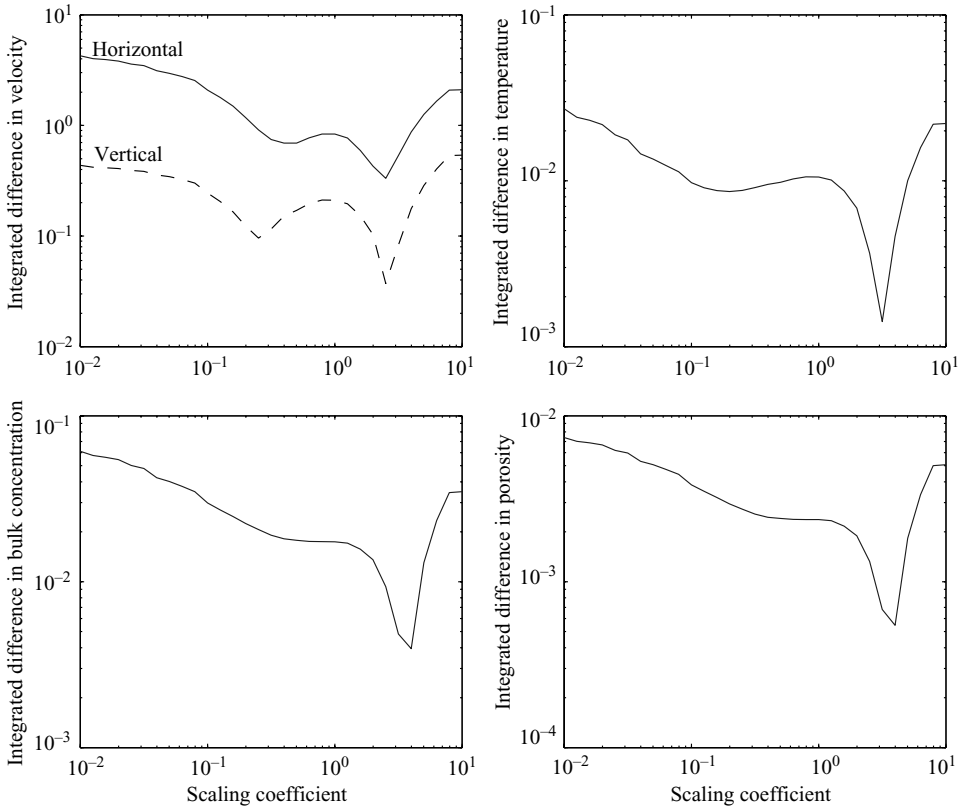

FIGURE 12. Integrated difference between the Darcy–Brinkman and the mixed Stokes–Darcy formulations with our interfacial conditions as a function of the scaling coefficient c ($V_{pull} = 1$, $V = 10$, $L = 10$, $Da = 10^{-4}$, $C_e/(C_\infty - C_e) = -7$, $m = 0.8$).

6. Conclusion

Studies of multiphase flows can be divided into two groups. Some models use a single Darcy–Brinkman formulation for both the liquid and the porous domains, and resolve the system on a single mesoscopic scale. Other models use independent sets of equations for the liquid and the porous matrix, with boundary conditions imposed at the sharp interface.

Previously suggested interfacial conditions, written directly at the porous matrix–liquid interface, do not give a satisfactory agreement with the Darcy–Brinkman results, even in the simple configurations studied here. Indeed, Darcy's equation does not take into account fluid–fluid viscous interactions that become important very close to the interface and/or when the permeability becomes large. We therefore define a viscous transition zone below the liquid–porous matrix interface, inside the porous matrix, where Stokes' law still applies, and consider Darcy's law only below it. This transition zone is of the order of the square root of the local value of the permeability divided by the liquid fraction. Using this formulation, a good agreement with the Darcy–Brinkman results is obtained, even for a continuous transition between liquid and solid, for instance during binary alloy solidification.

We must however keep in mind that the derivation of the mesoscopic volume-average Darcy–Brinkman equation necessitates many approximations. The study

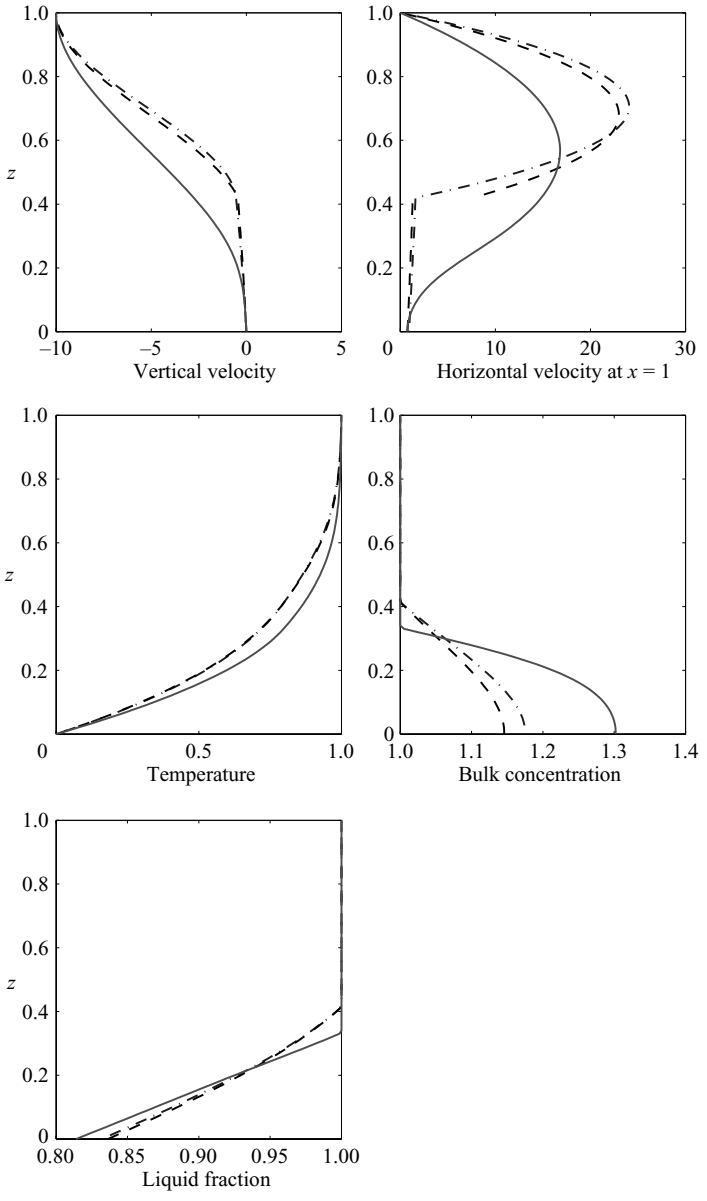

FIGURE 13. Comparison between steady-state profiles given by the Darcy–Brinkman formulation (continuous line) and the mixed Stokes–Darcy formulation using the non-divergent permeability function (5.14) and either a continuous horizontal velocity at the interface (dashed-dotted line) or Beavers & Joseph's (1967) interfacial conditions with $\alpha = 1$ (dashed line) for the solidification of a binary alloy in a corner flow ($V_{pull} = 1$, $V = 10$, $L = 10$, $Da = 10^{-4}$ corresponding to $\hat{\Pi}_0/h^2 = 2.9 \times 10^{-3}$, $C_e/(C_\infty - C_e) = -7$, $m = 0.8$).

here does not demonstrate its validity, which should be tested by careful experimental investigations (see also Zhao & Chen 2001). We suggest for instance reproducing Beavers & Joseph's (1967) experiments in the corner geometries studied here or investigating the precise macrosegregation patterns produced by binary alloy solidification, since this would simultaneously validate the Darcy–Brinkman equation

and test the various suggested interfacial boundary conditions in the Stokes–Darcy approach. The approach formulated and illustrated in this paper will allow systematic comparisons to be made between single-domain and sharp-interface models of alloy solidification; comparisons which may, in turn, indicate the need for better modelling of the interfacial regions of mushy zones.

The authors would like to acknowledge support from the Leverhulme Trust and from the European Community (Marie Curie Intra European Fellowship FP6-501040).

Appendix. The volume-averaging method

We consider a domain comprising both a solid and a liquid phase, for instance a porous medium or a solidifying material, and define a mesoscopic volume ΔV large enough to smooth the morphological complexities, but small enough to capture the global transport properties (i.e. typically a few pore lengths). At this intermediate scale, mesoscopic transport equations can be derived from the volume averaging of the microscopic equations over ΔV. Concepts and theorems that are used by this technique have been extensively studied (e.g. Gray 1975; Whitaker 1999) and are briefly recalled here for application to the momentum equation.

We define the liquid phase function ν_l by

$$\nu_l = \begin{cases} 1 & \text{in the liquid,} \\ 0 & \text{in the solid,} \end{cases}$$

and the liquid volume fraction (porosity) by

$$\chi = \frac{1}{\Delta V}\int_{\Delta V} \nu_l \,\mathrm{d}V = \frac{\Delta V_l}{\Delta V}, \tag{A 1}$$

where $\mathrm{d}V$ is an infinitesimal element of volume relative to the control volume ΔV and ΔV_l the volume of liquid contained in ΔV. The volume average of a given quantity of liquid per unit volume ϕ_l is

$$[\phi_l] = \frac{1}{\Delta V}\int_{\Delta V} \phi_l \nu_l \,\mathrm{d}V. \tag{A 2}$$

We also define the intrinsic volume average, i.e. the volume average in the liquid phase only,

$$[\phi_l]^l = \frac{1}{\Delta V_l}\int_{\Delta V} \phi_l \nu_l \,\mathrm{d}V = \frac{[\phi_l]}{\chi}, \tag{A 3}$$

and the fluctuating component

$$\hat{\phi}_l = (\phi_l - [\phi_l]^l)\nu_l. \tag{A 4}$$

We now introduce three useful mathematical formulae, valid when functions change on typical scales larger than the averaging length (Gray 1975; Whitaker 1999):

formula 1

$$[\phi_l \psi_l] = \chi [\phi_l]^l [\psi_l]^l + [\hat{\phi}_l \hat{\psi}_l], \tag{A 5}$$

where ψ_l is another given quantity of liquid per unit volume;

formula 2

$$\left[\frac{\partial \phi_l}{\partial t}\right] = \frac{\partial}{\partial t}[\phi_l] - \frac{1}{\Delta V}\int_{\Delta A} \phi_l \boldsymbol{w}\cdot\boldsymbol{n}_l \,\mathrm{d}A, \tag{A 6}$$

where ΔA is the interfacial area between the liquid and solid phases in ΔV, $\boldsymbol{w}$ is the velocity of the microscopic interface and $\boldsymbol{n}_l$ is the outward unit normal vector of the infinitesimal area $\mathrm{d}A$;

formula 3

$$[\nabla\phi_l] = \nabla[\phi_l] + \frac{1}{\Delta V}\int_{\Delta A}\phi_l \boldsymbol{n}_l \,\mathrm{d}A \tag{A 7}$$

which can also be written

$$[\nabla\phi_l] = \chi\nabla[\phi_l]^l + \frac{1}{\Delta V}\int_{\Delta A}\hat{\phi}_l \boldsymbol{n}_l \,\mathrm{d}A. \tag{A 8}$$

The demonstration of these three formulae is straightforward in the context of slowly variable functions, noting that

$$\frac{\partial v_l}{\partial t} = \begin{cases} \boldsymbol{w}\cdot\boldsymbol{n}_l & \text{on the liquid–solid interface,} \\ 0 & \text{elsewhere;} \end{cases}$$

$$\nabla v_l = \begin{cases} -\boldsymbol{n}_l & \text{on the liquid–solid interface,} \\ \boldsymbol{0} & \text{elsewhere.} \end{cases}$$

When functions change rapidly (i.e. over a length scale comparable to the averaging length, as for instance at a sharp porous matrix–liquid interface), a more complex approach is necessary (see for instance Ochoa-Tapia & Whitaker 1995*a*).

REFERENCES

Batchelor, G. K. 1967 *An Introduction to Fluid Dynamics*. Cambridge University Press.

Bear, J. 1972 *Dynamics of Fluids in Porous Media*. Dover.

Beavers, G. S. & Joseph, D. D. 1967 Boundary conditions at a naturally permeable wall. *J. Fluid Mech.* **30**, 197–207.

Beckermann, C., Diepers, H.-J., Steinbach, I., Karma, A. & Tong, X. 1999 Modeling melt convection in phase-field simulations of solidification. *J. Comput. Phys.* **154**, 468–496.

Beckermann, C. & Viskanta, R. 1988 Natural convection solid/liquid phase change in porous media. *Intl J. Heat Mass Transfer* **31**, 35–46.

Bennon, W. D. & Incropera, F. P. 1987 A continuum model for momentum, heat and species transport in binary solid–liquid phase change systems. *Intl J. Heat Mass Transfer* **30**, 2161–2171.

Brinkman, H. C. 1947 A calculation of the viscous force exerted by a flowing fluid on a dense swarm of particles. *Appl. Sci. Res.* A **1**, 27–34.

Chung, C. A. & Worster, M. G. 2002 Steady-state chimneys in a mushy layer. *J. Fluid Mech.* **455**, 387–411.

Cieszko, M. & Kubik, J. 1999 Derivation of matching conditions at the contact surface between fluid-saturated porous solid and bulk fluid. *Transport in Porous Media* **34**, 319–336.

Felicelli, S. D., Heinrich, J. C. & Poirier, D. R. 1991 Simulation of freckles during vertical solidification of binary alloys. *Metall. Trans.* B **22**, 847–859.

Gray, W. G. 1975 A derivation of the equations for multiphase transport. *Chem. Engng Sci.* **30**, 229–233.

Gu, J. & Beckermann, C. 1999 Simulation of convection and macrosegregation in a large steel ingot. *Metall Mat. Trans.* A **30**, 1357–1366.

Hills, R. N., Loper, D. E. & Roberts, P. H. 1983 A thermodynamically consistent model of a mushy zone. *Q. J. Mech. Appl. Maths* **36**, 505–539.

Kaempfer, T. U. & Rappaz, M. 2003 Modelling of macrosegregation during solidification processes using an adaptive domain decomposition method. *Modelling Simul. Mater. Sci. Engng* **11**, 575–597.

Lesieur, M. 1993 Numerical simulations of turbulence in shear flows. In *Advances in Turbulence IV* (ed. F. T. M. Nieuwstadt), pp. 345–351. Kluwer.

Levy, T. & Sanchez-Palencia, E. 1975 On the boundary conditions for fluid flow in porous media. *Intl J. Engng Sci.* **13**, 923–940.

Moin, P., Squires, K., Cabot, W. & Lee, S. 1991 A dynamic subgrid-scale model for compressible turbulence and scalar transport. *Phys. Fluids* A **3**, 2746–2757.

Neale, G. H. & Nader, W. K. 1974 Prediction of transport processes within porous media: Creeping flow relative to a fixed swarm of spherical particles. *AIChE J.* **20**, 530–538.

Ochoa-Tapia, J. & Whitaker, S. 1995*a* Momentum transfer at the boundary between a porous medium and a homogeneous fluid: I-theoretical development. *Intl J. Heat Mass Transfer* **38**, 2635–2646.

Ochoa-Tapia, J. & Whitaker, S. 1995*b* Momentum transfer at the boundary between a porous medium and a homogeneous fluid: II- comparison with experiment. *Intl J. Heat Mass Transfer* **38**, 2647–2655.

Saffman, P. G. 1971 On the boundary condition at the surface of a porous medium. *Stud. Appl. Maths* **L(2)**, 93–101.

Schneider, M. C., Gu, J. P., Beckermann, C., Boettinger, W. J. & Kattner, U. R. 1997 Modeling of micro- and macrosegregation and freckle formation in single-crystal nickel-base superalloy directional solidification. *Metall. Mater. Trans.* A **28**, 1517–1531.

Schulze, T. P. & Worster, M. G. 1999 Weak convection, liquid inclusions and the formation of chimneys in mushy layers. *J. Fluid Mech.* **388**, 197–215.

Shyy, W., Ouyang, H., Blosch, E., Thakur, S. S. & Liu, J. 1997 *Computational Techniques for Complex Transport Phenomena*. Cambridge University Press.

Whitaker, S. 1999 *The method of volume averaging*. Kluwer.

Worster, M. G. 1997 Convection in mushy layers. *Annu. Rev. Fluid Mech.* **29**, 91–122.

Worster, M. G. 2000 Solidification of fluids. In *Perspectives in Fluid Dynamics* (ed. G. K. Batchelor, H. K. Moffat & M. G. Worster), pp. 393–446. Cambridge University Press.

Zhao, P. & Chen, C. F. 2001 Stability analysis of double-diffusive convection in superposed fluid and porous layers using a one-equation model. *Intl J. Heat Mass Transfer* **44**, 4625–4633.